THE ENERGETICS OF MOLECULAR CLOUDS. I. METHODS OF ANALYSIS AND APPLICATION TO THE S255 MOLECULAR CLOUD

N. J. EVANS II*†
Department of Astronomy and McDonald Observatory, University of Texas at Austin

GUY N. BLAIR†
Department of Astronomy and McDonald Observatory, University of Texas at Austin,
and Netherlands Foundation for Radio Astronomy

S. BECKWITH
Department of Physics, California Institute of Technology

ABSTRACT

This paper is the first of a series that result from a program to collect complete molecular line, radio continuum, and infrared data on a group of relatively simple, nearby molecular clouds. These data are used to determine the physical properties of the molecular clouds and to analyze the energetic relationship between the gas and the dust in the clouds. The analysis includes estimates of the kinetic temperature, gas density, gas cooling rate, and dust cooling rate. The cooling rates are then compared to relevant heating rates from collapse, and from radiative heating by nearby stars and embedded infrared sources. In this paper, the methods of analysis are described and applied to the molecular cloud associated with S255. The most salient results are the following: (1) The primary energy flow is through the dust, which is cooled by far-infrared radiation. (2) The gas cooling rate is much less than the dust cooling rate. (3) The primary heat sources appear to be nearby stars, but an embedded infrared source is responsible for at least local heating. (4) There is a strong enhancement of molecular density, as well as temperature, centered on the embedded infrared source. (5) A large far-infrared flux ($\sim 10^3$ Jy) is predicted. (6) Suitable far-infrared and submillimeter measurements of this cloud would provide strong tests of molecular cloud models in which the gas is heated by collisions with dust.

Subject headings: interstellar: molecules — infrared: sources — nebulae: general — radio sources: general — radio sources: lines

I. INTRODUCTION

The fact that thermal molecular line emission, far-infrared dust emission, compact near-infrared (5–20 μm) sources, compact H II regions, and OH and H_2O masers are often found in close combination is by now well established. Further, it is generally accepted that these phenomena are indications that star formation has occurred recently or is now proceeding. Some effort has also been made to formulate a general theoretical framework for analysis of these objects (Goldreich and Kwan 1974; Scoville and Kwan 1976; Leung 1976). Nonetheless, there are few satisfactory applications of basic theory to the wealth of observational material that is now available. We have attempted to remedy the situation by collecting as complete a set of data as possible on a selected group of relatively simple objects and by developing and applying "first-order" techniques of analysis in order to establish parameters which can be used to construct more sophisticated models.

The objects were selected from a CO survey (Blair, Peters, and Vanden Bout 1975; Blair 1976) of small Hα emission regions. The choice of objects for more detailed study was influenced by the following criteria:

1. The clouds are less complex geometrically than the previously studied clouds.

2. A good distance measurement is available and the clouds are relatively close (< 2 kpc).

3. High-angular-resolution radio continuum maps are available; these maps can be used to determine the properties and positions of compact H II regions.

4. The CO emission peak is unambiguously associated with a single, strong, compact near-infrared source. Thus, *at least* the region of peak CO emission should be energetically related to the near-infrared source, rather than to nearby H II regions and their exciting stars.

These criteria defined the objectives; not all the criteria were satisfied completely in any region. Ideally, we would like to study regions with only a near-infrared source and no nearby H II regions or luminous stars, so that the effects of the near-infrared source on the energetics of the whole molecular cloud could be more easily studied. Unfortunately, no such regions have

448

been found; as a substitute, clouds where the exciting stars are less luminous or farther removed have been used. In this paper we will outline the techniques of analysis and apply them to the molecular cloud associated with S255 (IC 2162). In a companion paper (Blair *et al.* 1977), these techniques will be applied to the molecular cloud associated with S140.

The S255 molecular cloud is a region of extended CO emission associated with a cluster of red nebulae, denoted S254–S257 by Sharpless (1959). The radio continuum emission from these objects has been studied at various wavelengths. High-resolution continuum maps are available at 21 cm and at 6 cm wavelengths for the regions S255–S257 (Israel 1976). Both an OH (Turner 1971) and an H_2O maser (Lo and Burke 1973) have been detected in this region. There is some uncertainty about the distance to this complex. The kinematic distance, from both molecular emission and $H\alpha$ measurements, is 0.8–1.3 kpc; but studies of two of the exciting stars suggest a distance of 3 kpc (Israel 1976). Because there is some question about the latter determination, we will adopt 1 kpc as the distance to the object.

In the next two sections, we will outline our molecular and infrared observations and results. In §§ IV and V, the adopted methods of analysis are described and applied to the S255 molecular cloud. Section IV is devoted to a discussion of the physical conditions in the cloud (temperature, molecular column density, hydrogen volume density). These properties will be derived from molecular line observations of CO, ^{13}CO, and H_2CO. Section V contains a discussion of heating and cooling rates for the gas and dust and of the cloud energetics. The gas cooling rates will be derived from the CO observations. Those observations will also yield an estimate of the dust cooling rates. The heating rates for the dust will then be determined from near-infrared observations and the properties of the exciting stars of the H II regions. Section VI will discuss observational consequences of the picture developed in §§ IV and V.

II. OBSERVING TECHNIQUES

a) Molecular Line Observations

Most of the $^{12}C^{16}O$(CO) and $^{13}C^{16}O$(^{13}CO) data and all of the data on the $H_2^{12}C^{16}O$ $2_{12} \rightarrow 1_{11}$ transition (2 mm H_2CO) were collected at the 5 m antenna of the Millimeter Wave Observatory (MWO), at Fort Davis, Texas.[1] The receiver was operated in the frequency-switched mode and the single-sideband system temperature varied from 1500 K to 3000 K from run to run. At the frequency of the 2 mm H_2CO line, the system temperature was 1600–2000 K. The velocity resolution, velocity coverage, and half-power beamwidth are given in Table 1 for each transition. The chopper wheel calibration method was used, and relative calibration was improved by measuring the central position of the S255 cloud several times during each session. OMC-1 was measured at least once per day to improve absolute intensity calibration. The errors for the CO and ^{13}CO data from MWO are conservatively estimated at 15%–25% for line strengths, 0.7 km s^{-1} for radial velocities, and 1' for absolute positions.

For the 2 mm H_2CO observations, the ambient temperature was monitored and the atmospheric opacity was determined 2 to 3 times daily, depending on weather conditions. Observations of OMC-1 indicate that calibration uncertainties are $\pm 10\%$ or less; errors for velocities are estimated to be 0.5–1.0 km s^{-1}, and errors for absolute positions are $\pm 30''$.

To achieve higher resolution in space and velocity, we obtained additional observations of CO and ^{13}CO at the 11 m telescope of the National Radio Astronomy Observatory[2] at Kitt Peak. Pointing and velocity errors are estimated to be 10'' and 0.26 km s^{-1}, respectively.

Observations of the $2_{11} \leftarrow 2_{12}$ (2 cm) and $1_{10} \leftarrow 1_{11}$ (6 cm) transitions of $H_2^{12}C^{16}O$ were obtained at the 43 m telescope of the NRAO, in Green Bank. The autocorrelator back end was operated with an effective resolution of 0.26 km s^{-1} and a total velocity range of 21 km s^{-1}. The half-power beamwidths are 2' at 2 cm and 6' at 6 cm. The pointing errors should be 0.5 at 6 cm and 0.3 at 2 cm. The 6 cm efficiency for extended sources is 0.80. The 2 cm efficiencies for extended and small (15'') sources were taken from Kutner, Evans, and Tucker (1976) as 0.67 and 0.42, respectively. The calibration errors should be no larger than $\pm 5\%$. For a more complete discussion of

TABLE 1
MWO OBSERVING PARAMETERS

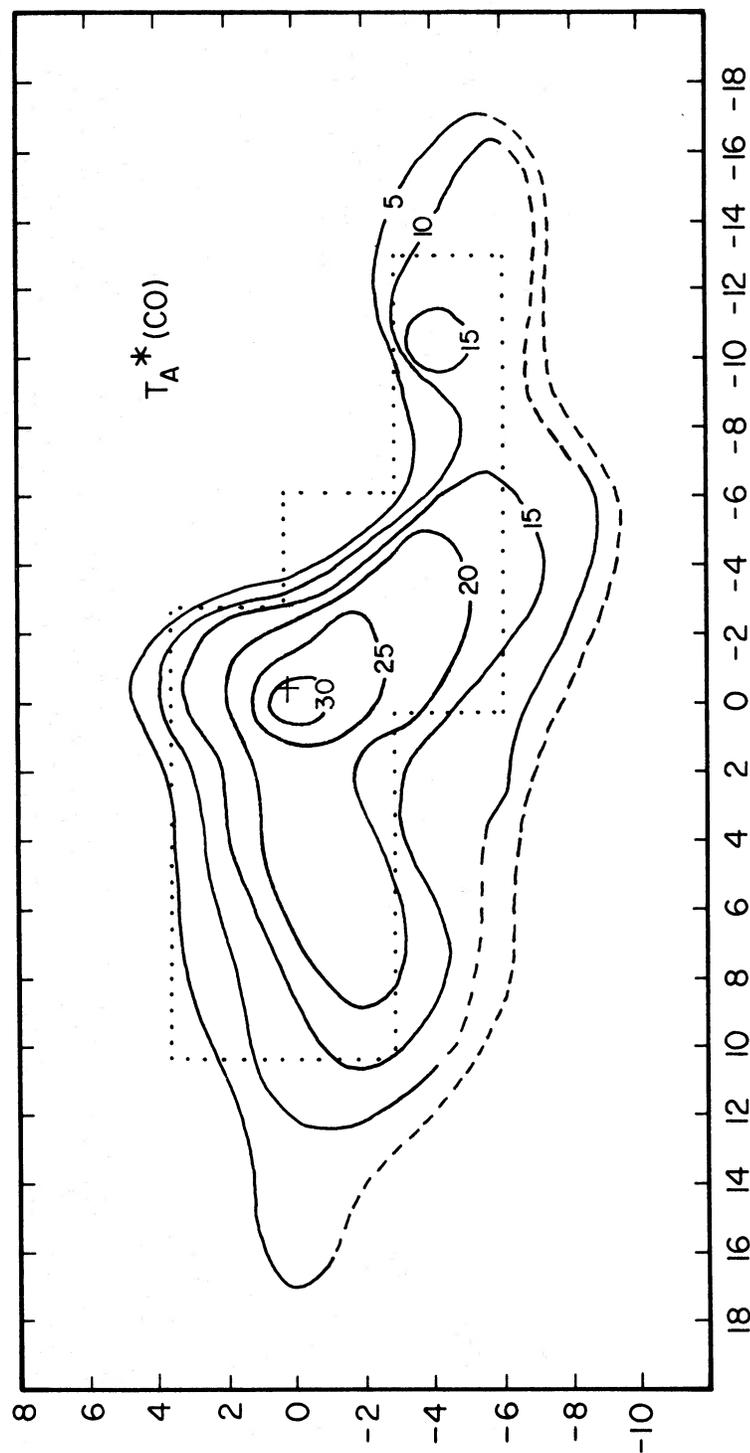| Molecule (1)	Frequency (MHz) (2)	Beam (arcmin) (3)	Velocity Resolution (km s^{-1}) (4)	Velocity Coverage (km s^{-1}) (5)
CO..........	115271.201	2.3	0.65	26.0
^{13}CO.......	110201.370	2.3	0.68	27.2
H_2CO.......	140839.53	1.8	0.53	21.3

Fig. 1.—Contour map of T_A^*, the corrected antenna temperature of CO, in the S255 molecular cloud. The offsets are in minutes of arc with respect to the position, with 1950 coordinates of $\alpha = 06^h10^m01^s$ and $\delta = +18°00'00''$. This position is at $l^{II} = 192$, $b^{II} = 0$. The dotted line indicates the region mapped at 2 μm, and the plus sign indicates the position of S255 IR.
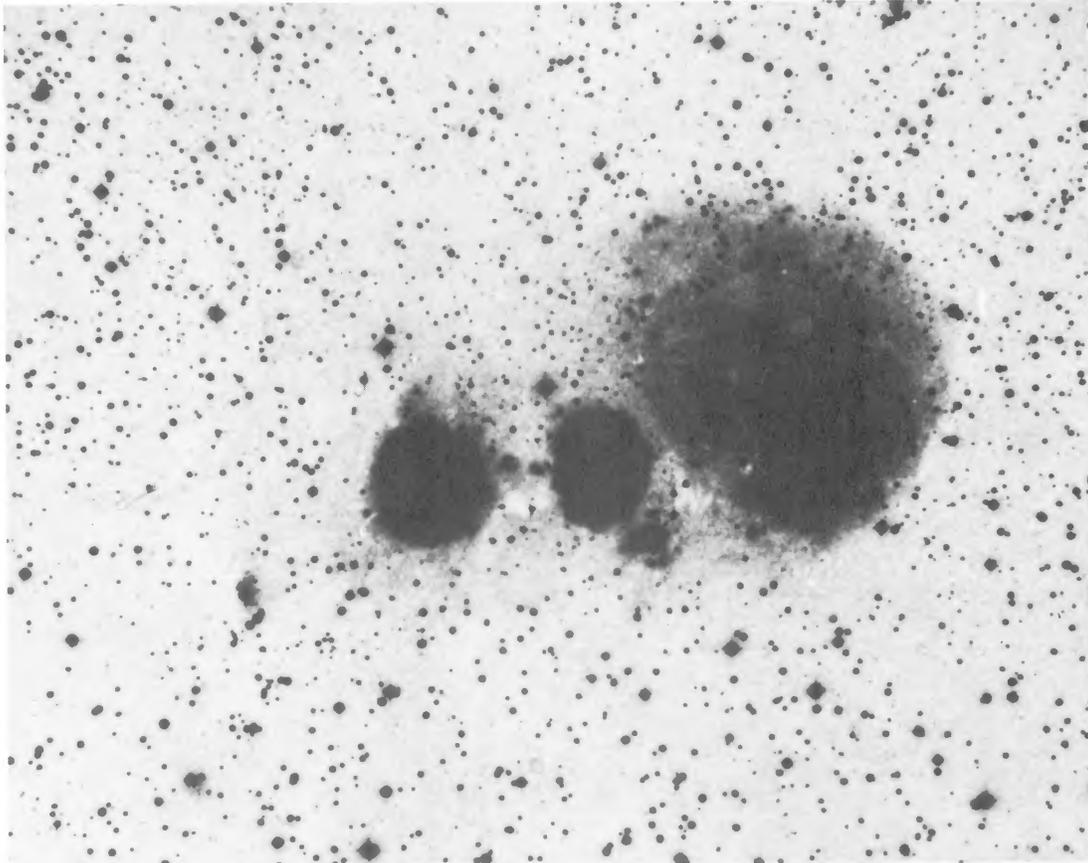
450

FIG. 2.—Visual appearance of the region, taken from the red print of the Palomar Sky Survey. The scale is *similar* to those of Figs. 1, 3, and 6.

the molecular line observing techniques, see Blair (1976).

b) Infrared Observations

The region of enhanced CO emission was mapped at 2.2 μm with the 1.3 m telescope of the Kitt Peak National Observatory. The basic system and mapping procedures are those described by Strom, Strom, and Vrba (1976). A 63″ beam was used with a 50″ chopper spacing. A grid of points separated by 50″ was mapped with an integration time of 16 s per point. This method was used only to find sources, not for photometry. Seven sources were found which are stronger than 0.1 Jy at 2.2 μm. Positions and photometry from 1.2 to 3.4 μm were obtained for these sources by using a 30″ aperture and 50″ chopper spacing, allowing accurate photometry on the sources found with the larger beam. Before the photometry, the source signal was peaked up in a 10″ or 15″ aperture, and afterward the position of the source relative to a field star was measured. For the strong 10 μm infrared source, S255 IR, multicolor photometry was obtained at four different aperture sizes.

The 1.5 m telescope of the Mount Wilson Observatory was used to obtain the data on the strong 10 μm source, S255 IR, presented in Figure 5. The equipment and techniques are those described by Beckwith et al. (1976). The photometry at 2.2–4.8 μm and at 20 μm was done with a 9″ beam and a 18″ chopper spacing. The photometry in the four filters around 10 μm was done with an 8″ beam and a 14″ spacing; the large errors on these data are due to overall calibration uncertainties; the relative fluxes in the four filters have much lower errors. An accurate position for the source was determined by measuring its position relative to several nearby faint stars, whose positions were then measured from the Palomar Sky Survey plate.

III. RESULTS

a) CO and ^{13}CO

The ^{12}CO (henceforth denoted CO) data are presented in Figure 1 in the form of contours of T_A^*, the antenna temperature corrected for atmospheric and antenna ohmic losses. The contours are based on data of 2.′3 resolution taken at 2′ spacings at MWO, except near the peak, where some data with 1′ resolution from the NRAO 11 m antenna have been used to define the two strongest contours. The dashed lines indicate regions of inadequate spatial coverage. The CO map shows strong, extended emission peaking in the obscured region about 2′ west of the nebula S255. The offsets on this and subsequent maps are with respect to the position with 1950 coordinates of $\alpha = 06^h10^m01^s$ and $\delta = +18°00'00''$, a position close to the CO peak. The velocity of peak emission is 7.8 km s^{-1}; the velocity seems to increase slightly both in the extreme east and in the southwest, but no other

systematic trends in velocity are apparent. Emission at 7.8 km s^{-1} clearly extends behind the visible nebulae, S255–S257, but cuts off sharply at the southeast boundary of the largest visible nebula, S254 (cf. Fig. 2). Just at that point, emission in two other velocity features at ~ 0 km s^{-1} and at ~ 24 km s^{-1} becomes visible and extends over the region of S254. This emission is not shown in Figure 1. The line width of the 7.8 km s^{-1} feature exhibits a mild peaking in the region of peak T_A^*. From a maximum value (full width at half-maximum) of 4 km s^{-1} it drops to 2–3 km s^{-1} within 4′–6′ to the north, east, and south. The line width remains large in the region that extends to the southwest. The CO data taken around the peak with the 11 m telescope show no enhanced line broadening or extended line wings associated with the infrared source.

The ^{13}CO results are presented in Figure 3 as a grid of numbers representing peak T_A^*. The 21 cm radio contours of Israel (1976) are indicated for comparison. While the ^{13}CO map is less extensive, it is qualitatively similar to the CO map in showing a sharp cutoff near the boundary of S254, a relatively rapid decline to the north of the peak, and a broad plateau in the southwest. The peak of $T_A^*(^{13}$CO) appears to be 1′–2′ south of the CO peak. The ^{13}CO velocities tend to be slightly lower than the ^{12}CO velocities, especially in the southwest plateau, while the variations in line width are similar to those in ^{12}CO. The compact radio source G192.58 − 0.04 lies 2′ northwest of the position of peak T_A^*. This compact source has no observable effect on the CO or ^{13}CO emission intensity or line width.

b) H$_2$CO

The results from the 6 cm H$_2$CO observations are presented in Table 2. The offsets are with respect to the reference position of the CO map: $\alpha(1950) = 06^h10^m01^s$; $\delta(1950) = +18°00'00''$. The 2 cm and 2 mm data are presented in Table 3, where the offsets follow the same convention. The intensity of the 6 cm and 2 cm lines is given as T_A/η, where η is the efficiency of the 43 m telescope for an extended source at the appropriate wavelength. The 2 mm intensity is given as T_A^*.

The 6 cm absorption is widespread; when we consider the 6′ beam, the absorption appears to cover essentially the entire region of the CO map. The rather

TABLE 2
6 CENTIMETER FORMALDEHYDE RESULTS

Offset (arcmin)	T_A/η^* (K)	V_{LSR} (km s^{-1})	ΔV (km s^{-1})
....	−0.14 (0.03)	6.4	1.8
6′ E............	−0.09 (0.03)	7.1	4.0
6′ S............	−0.16 (0.04)	6.4	2.8
6′ W, 6′ S......	−0.19 (0.03)	7.0	2.8
6′ W, 12′ S....	−0.19 (0.04)	6.4	3.3
14′ E, 6′ S.....	−0.25 (0.05)	8.4	2.4

* $\eta = 0.80$; 1 σ errors are given in parentheses.

TABLE 3

FORMALDEHYDE RESULTS

Offset (arcmin) (1)	2 Centimeter			2 Millimeter		
	T_A/η† (K) (2)	V_{LSR} (km s^{-1}) (3)	ΔV (km s^{-1}) (4)	T_A^* (K) (5)	V_{LSR} (km s^{-1}) (6)	ΔV (km s^{-1}) (7)
....	−0.03 (0.015)	5.8	2.8	1.7 (0.3)	8.0	2.3
4′ E.........	−0.04 (0.025)	7	∼1	...	...	...
2′ E.........	−0.05 (0.025)	6.4	1.0	0.4 (0.2)	7.1	1.5
4′ N.........	...	...	...	0.5 (0.2)	6.2	1.3
2′ N.........	...	...	...	1.2 (0.3)	8.5	2.8
2′ S.........	...	...	...	1.2 (0.3)	7.3	0.8
2′ W.........	<0.03	...	...	0.5 (0.2)	7.4	2.0
6′ W, 6′ S....	<0.05	...	...	...	...	...

†$\eta = 0.67$; 1 σ errors are given in parentheses.

uniform strength of absorption over the map indicates that the H_2CO is absorbing the cosmic background radiation rather than the continuum radiation. The 2 cm and 2 mm maps are less extensive and are concentrated around the region of the CO peak. Emission in the 2 mm line, while confined to a small region around the CO peak, is clearly extended in the north-south direction, and is probably also extended east-west.

c) Infrared

The area mapped at 2.2 μm is indicated by the boxed-in area in Figure 1. Within this area, seven sources with 2.2 μm fluxes ≥ 0.1 Jy were found; one of these is the strong 10 μm infrared source found independently by Pipher and Soifer (1976) based on the H_2O maser position of Lo and Burke (1973). This source, denoted S255 IR, is discussed in detail below. The other six sources are not very red ([1.66 μm] − [2.22 μm] < 0.8) and do not coincide with any features in the CO map. Photometry of these sources is presented in Table 4, along with positions; the photometry suggests that none of these sources represents a significant source of heating for the cloud.

The position of the infrared source, marked by a plus sign on the CO contour map (Fig. 1), is $\alpha(1950) = 06^h09^m58^s4$; $\delta(1950) = +18°00'12''$, with errors of $\pm 4''$ in both coordinates. This position is very near the CO peak and the position of strongest 2 mm H_2CO emission. The infrared source also lies within the error boxes of the OH maser (Evans, Crutcher, and Wilson 1976) and the H_2O maser, but does not coincide with the compact radio continuum source G192.58−0.04, as can be seen in Figure 4, a reproduction of the 6 cm continuum map from Israel (1976). The upper limit at the infrared position (<3 mJy at 6 cm) indicates that any star with an H II region which is optically thin at 6 cm must have a spectral type later than ∼B1.

The energy distribution of S255 IR is shown in Figure 5. The fact that the energy distribution peaks around 5–20 μm and the existence of a 10 μm absorption feature identify S255 IR as a member of the class

of compact near-infrared sources without radio continuum emission, the most famous example of which is the Becklin-Neugebauer object. We have determined a color temperature of 435 K from the 12.5 and 3.4 μm points, and a blackbody of this T_c is represented by the dashed line in Figure 5. Pipher and Soifer (1976) have obtained high-resolution data in the silicate feature and have fitted their data with $3.7 < \tau_{sil} < 5.6$.

A series of measurements of S255 IR, made with different apertures on the 1.3 m telescope, are presented in Table 4. The source appears to become much redder as the aperture size is decreased. Quantitatively, the color from 3.45 to 1.66 μm changed by 1.2 mag when the aperture was decreased from 32″ to 16″.
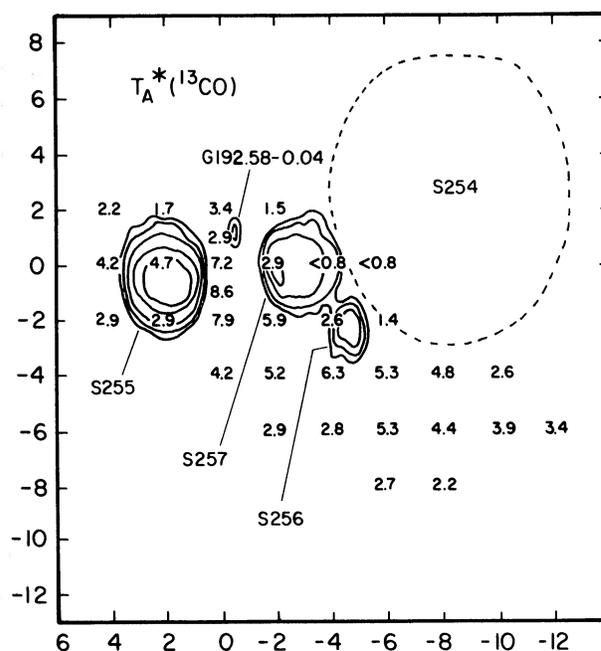
FIG. 3.—Peak T_A^* of ^{13}CO, superposed on the 21 cm radio continuum contours of Israel (1976). The offsets follow the same convention as in Fig. 1. The dashed contour indicates roughly the outer boundary of S254, which is overresolved in the 21 cm radio map.

TABLE 4

PHOTOMETRY* OF INFRARED SOURCES

No.	α(1950)	δ(1950)	Aperture arcsec	J 1.23 μm	H 1.66 μm	K 2.22 μm	L 3.45 μm	M 4.60 μm
1.........	$06^h09^m49^s5 \pm 15''$	$17°59'56'' \pm 15''$	32	0.30 (0.01)	0.21 (0.01)	0.13 (0.01)	< 0.12 (3σ)	
2†........	06 09 54.5 ± 10″	18 02 32 ± 10″	32	0.95 (0.05)	0.88 (0.04)	0.55 (0.03)	0.23 (0.04)	
3.........	06 10 04.6 ± 10″	18 03 20 ± 10″	32	0.050 (0.003)	0.17 (0.01)	0.19 (0.01)	< 0.13 (3σ)	
4.........	06 10 28.3 ± 10″	18 02 20 ± 10″	32	0.40 (0.02)	1.13 (0.06)	1.24 (0.06)	0.96 (0.06)	
5.........	06 09 40.7 ± 15″	17 56 55 ± 15″	32	0.092 (0.005)	0.10 (0.01)	0.10 (0.01)	< 0.15 (3σ)	
6.........	06 09 30.5 ± 10″	17 54 50 ± 10″	32	0.34 (0.02)	0.26 (0.02)	0.17 (0.01)	< 0.28 (3σ)	
S255 IR....	06 09 58.4 ± 4″	18 00 12 ± 4″	32	0.11 (0.01)	0.19 (0.005)	0.48 (0.02)	4.10 (0.21)	22.7 (2.3)
			23	0.033 (0.007)	0.086 (0.005)	0.31 (0.02)	3.47 (0.17)	19.1 (1.9)
			16	< 0.017 (3 σ)	0.046 (0.005)	0.20 (0.01)	3.09 (0.16)	17.0 (1.7)
			11	< 0.017 (3 σ)	0.030 (0.005)	0.15 (0.01)	2.84 (0.14)	17.1 (1.7)

* All photometric results are given in Jy; 1 σ errors are given in parentheses and are often due to calibration uncertainties, taken to be ±5% at *J–L* and ±10% at *M*.

† Visible star at this position.

These data show that another source must be present within a 30″ beam or that an extended source exists in this region. The 6 cm radio continuum map indicates that a weak continuum source, G192.60−0.04, lies 18″ E and 4″ N of S255 IR (see Fig. 4). Preliminary mapping suggests that the excess emission seen in large apertures may come from the position of this source, but more sensitive maps with small beams are necessary.

IV. PHYSICAL CONDITIONS IN THE MOLECULAR CLOUD

In this section we will use the CO, ^{13}CO, and H_2CO observations to establish the kinetic temperature, the
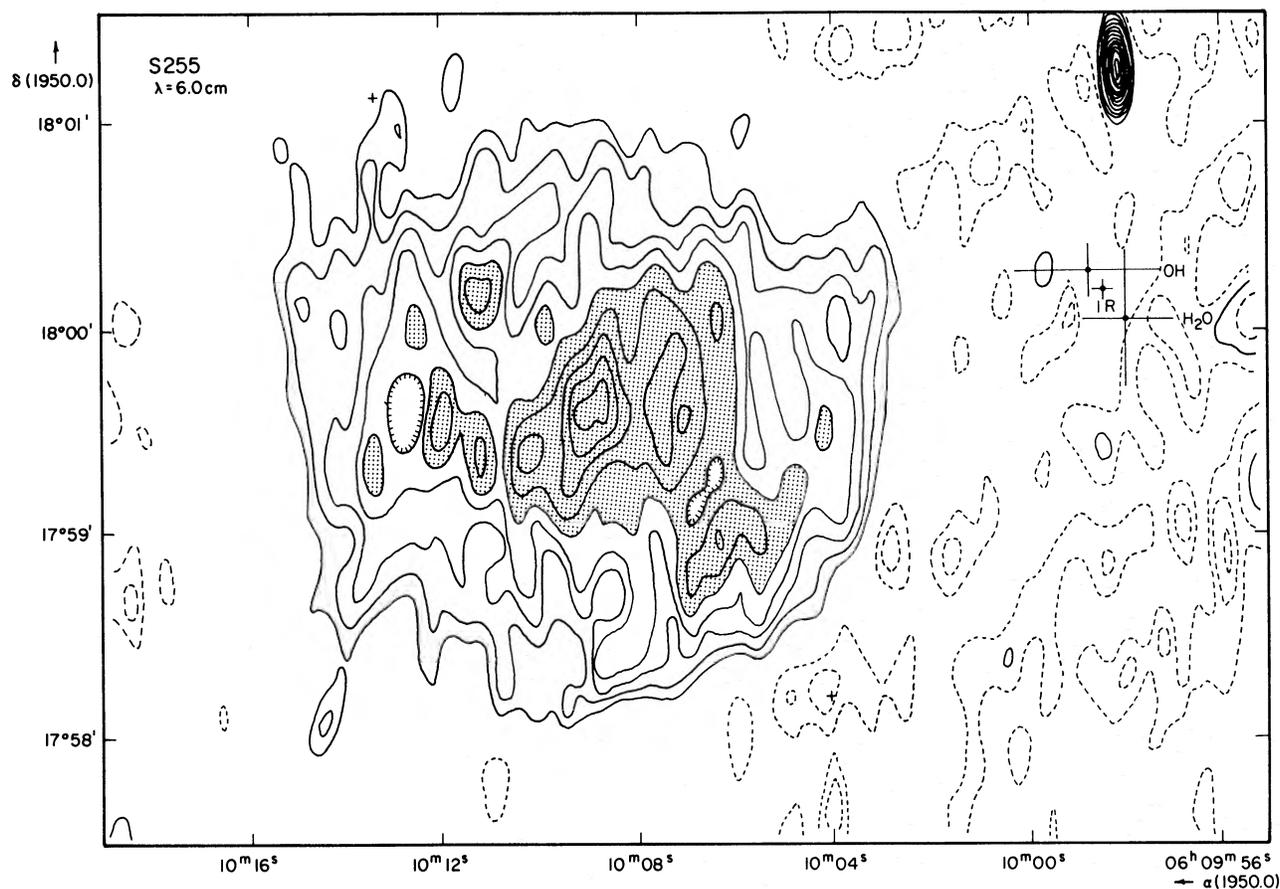

FIG. 4.—Reproduction of the 6 cm radio continuum contours of S255 from Israel (1976), with the positions of S255 IR and the OH and H_2O masers marked. Note that the scale is expanded compared with other figures.

TABLE 5
CLOUD PARAMETERS

Ring No. (1)	$T_A*(CO)$ (K) (2)	a_i (pc²) (3)	T_K (K) (4)	l_i (pc) (5)	$\Lambda_{CO}\Delta v_i$ ($L_\odot$) (6)	C_i(FIR) ($L_\odot$) (7)
1..........	30	0.15	33.5	0.44	2.2×10^{-2}	3.5×10^3
2..........	25	0.83	28.5	1.03	1.7×10^{-1}	5.7×10^3
3..........	20	4.02	23.5	2.27	9.6×10^{-1}	1.3×10^4
4..........	15	7.31	18.5	3.02	7.2×10^{-1}	8.9×10^3
5..........	10	13.16	13.3	4.10	6.9×10^{-1}	4.3×10^3

density, and the mass of the molecular cloud. In addition, the column density of ^{13}CO will be derived because it will be used in § V during the discussion of dust energetics to estimate the far-infrared optical depth of the dust.

a) Geometrical Assumptions

In order to derive the physical conditions in the cloud, such as density, temperature, and mass, it is usually necessary to make some assumption about the geometry of the region. In the following sections we shall take, as the primary *observed* geometrical information, the area interior to a given contour level on the map of $T_A*(CO)$. Accordingly, these areas (a_i) have been measured from Figure 1 and are given in column (3) of Table 5. These a_i are then assumed to be the projected area of a three-dimensional region with a surface area, $s_i = 4 \times a_i$, a volume $v_i = 0.75a_i^{3/2}$, and a path length through the center of $l_i = 1.13a_i^{1/2}$. The coefficients have been chosen to make these expressions correct for a spherical region. Even in the extreme case of a thin slab, s_i will be only a factor of 2 less than the above value, but the volume and path length may of course be quite wrong. Finally, these regions are assumed to form a series of concentric shells after the manner of an onion, each with uniform properties.

b) Kinetic Temperature

The determination of gas kinetic temperature, T_K, is probably the most straightforward technique. For a region of uniform T_{ex} along the line of sight, T_A* is given by

$$T_A* = \eta_p[f_\nu(T_{ex}) - f_\nu(T_{bg})][1 - e^{-\tau}],   (1)$$

where

$$f_\nu(T) = \frac{h\nu}{k}[e^{h\nu/kT} - 1].$$

T_{ex} is the excitation temperature of the line, T_{bg} is the brightness temperature of the background radiation, and η_p corrects for both filling factor and part of the antenna efficiency. For CO, we take $\eta_p = 1$, $T_{ex} = T_K$, and $\tau = \infty$; the derived T_K (col. [4] of Table 5) at the peak is 34 K, falling off to 13 K at the $T_A* = 10$ K contour. The question of how one "sees into" the region of $T_K = 34$ K through an optically thick outer

shell of $T_K = 13$ K may be answered by reference to large velocity gradients (see Goldreich and Kwan 1974; Scoville and Solomon 1974) or by a clumpy cloud model (see Zuckerman and Evans 1974). Either of these models will allow one to see past a region of high optical depth but low temperature into a higher-temperature region. However, the possibility that regions of even higher temperature are hidden inside the cloud should not be forgotten.

c) Molecular Column Density

The determination of the column density of the cloud is less standardized. We have chosen to express this parameter in terms of $n_{13}L$, the column density of ^{13}CO. Again, there are conflicting methods for de-
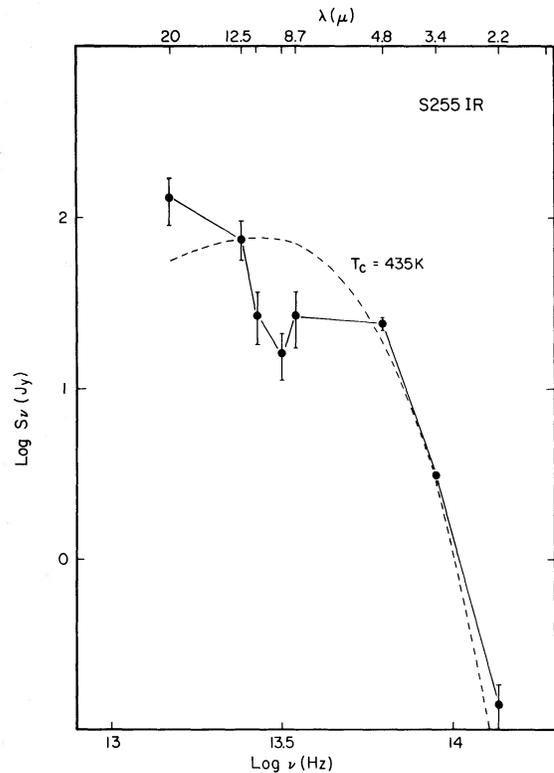

FIG. 5.—The energy distribution of S255 IR. The dotted line is a blackbody curve at $T_c = 435$ K, the color temperature derived from the 12.5 and 3.4 μm fluxes.
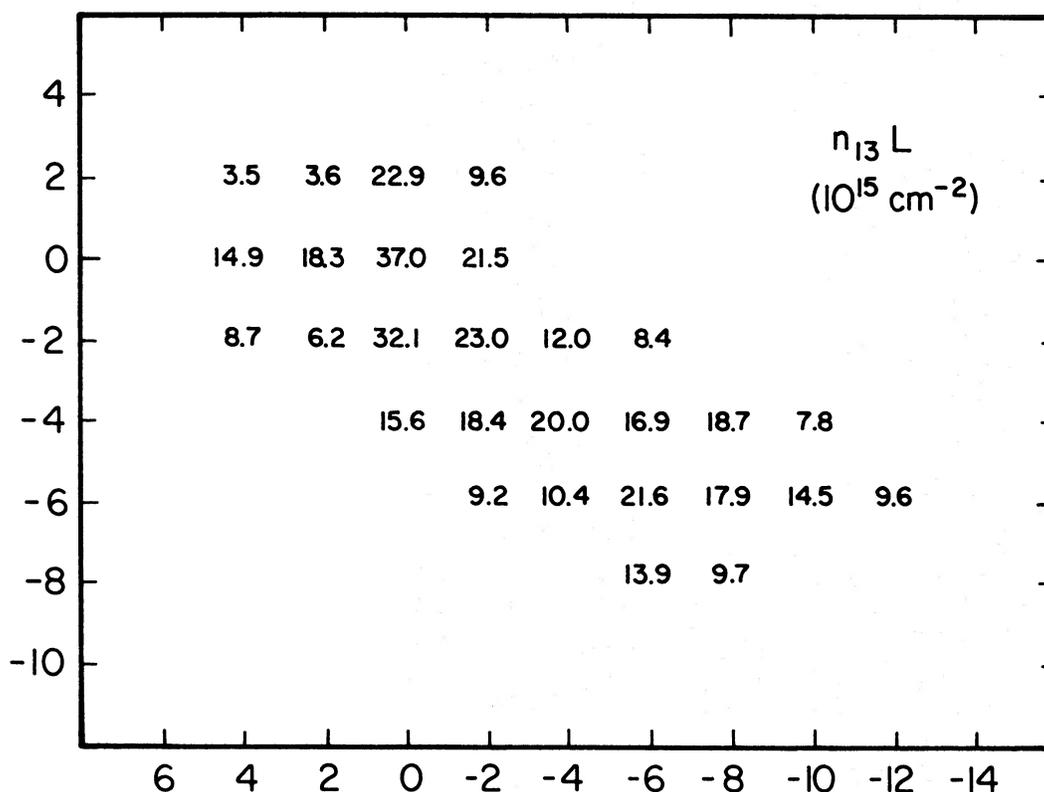
FIG. 6.—Column density of ^{13}CO ($n_{13}L$) in units of 10^{15} cm^{-2}. The offsets follow the same convention as in Fig. 1. These numbers are larger than would be derived from eq. (2) by a factor of 1.27, owing to the use of an incorrect value for the CO dipole moment. While this error is negligible compared to the uncertainties, we note it for the sake of consistency.

termining this quantity; we have chosen one in which the assumptions are few and explicit. The full derivation is given in Appendix A of Blair (1976), but the basic assumptions are the following: (1) the region is uniform along the line of sight and across the beam; (2) CO is optically thick and ^{13}CO is optically thin; and (3) $f_\nu(T_{ex}^{13}) \gg f_\nu(T_{bg})$, where T_{ex}^{13} is the excitation temperature of the $J = 1 \rightarrow 0$ transition of ^{13}CO. With these assumptions,

$$n_{13}L = 3.6 \times 10^{14}\Delta V(\text{km s}^{-1})T_A*(^{13}CO)/f_1, \quad (2)$$

where f_1 is the fraction of ^{13}CO molecules in the $J = 1$ state. In this method, no assumption about equal excitation temperatures of CO and ^{13}CO is made. The factor f_1 includes the effects of excitation and trapping; f_1 approaches the value of 0.26 at high densities ($\gtrsim 10^4$ cm^{-3}) of hydrogen (n_{H_2}); and $0.26 < f_1 < 0.55$ for $n_{H_2} > 10$ cm^{-3} (Blair 1976). The map of $n_{13}L$ (Fig. 6) was made by application of equation (2) to the ^{13}CO data with the assumption $f_1 = 0.26$. This value of f_1 may result in an overestimate of $n_{13}L$ by a factor less than ~ 2 in the outer regions of the cloud, but should be quite good in the inner regions. The map of $n_{13}L$ peaks at the CO peak, and declines away from the peak somewhat more rapidly than the CO or ^{13}CO T_A* maps, reflecting the fact that both ΔV and $T_A*(^{13}CO)$ decline away from the peak.

d) Hydrogen Volume Density and Mass

A variety of methods may be used to determine n_{H_2}, the hydrogen volume density. In the denser region of the cloud, the excitation of H_2CO provides a direct measure of n_{H_2}. Using the 2 mm emission line with the 2 cm absorption line, one can resolve the ambiguity created by trapping (Evans and Kutner 1976). At the position of peak H_2CO emission, the solution for n_{H_2} is 2×10^5 cm^{-3}. This result is based on calculation of the peak line temperatures in a large velocity gradient (LVG) trapping code.

Outside the dense region where H_2CO emission is seen, only an indirect determination of n_{H_2} is possible. In this method, one relates $n_{13}L$ to $n_{H_2}L$ and assumes a value for L. We take

$$n_{H_2}L = 5.0 \times 10^5 \times n_{13}L \quad (3)$$

from Dickman (1976); this value was determined by comparing visual extinction to ^{13}CO column density in dark dust clouds. We find that $n_{H_2}L = 1.9 \times 10^{22}$ cm^{-2} through the peak, falling to $n_{H_2}L \sim 3 \times 10^{21}$ cm^{-2} around the edges of the map. An average over all 28 measurements of $n_{13}L$ gives $\langle n_{H_2}L \rangle = 7.6 \times 10^{21}$ cm^{-2}. We take L equal to l_i for the $T_A*(CO) = 15$ K contour; with this value of $L = 3.0$ pc, we find n_{H_2} falls from 2×10^3 cm^{-3} at the peak to 4×10^2 cm^{-3} around the edges; using $\langle n_{H_2}L \rangle$ above gives

$\langle n_{H_2} \rangle \sim 8 \times 10^2$ cm^{-3}. Values of $n_{H_2} \sim 10^3$ cm^{-3} are in rough agreement with minimum densities required to excite CO and to explain the widespread anomalous absorption by H_2CO at 6 cm (see Evans *et al.* 1975).

The total mass of the cloud may be estimated by multiplying $\langle n_{H_2} L \rangle$ by the projected area, a_t, of the 10 K contour of $T_A{}^*$(CO). The result is $M = 1.5 \times 10^3$ $M_\odot$; note that this mass is incorrect in Table III-2 of Blair (1976). The total mass based on the virial theorem is 5×10^3 $M_\odot$.

At the peak position, the direct estimate of n_{H_2} from considerations of H_2CO excitation is 10^2 larger than the indirect estimate. This fact suggests an examination of the possible errors in the indirect method. The assumptions used to calculate n_{H_2} from the ^{13}CO data are the following: those used to derive $n_{13}L$; the use of equation (3) for $n_{H_2}L$; and that L is equal to l_i for the 15 K contour of $T_A{}^*$(CO). While it is hard to evaluate the likelihood that the cloud is much smaller along the line of sight than transverse to the line of sight, it seems unlikely that this effect could alone account for the large discrepancy. It should also be noted that if the cloud is really at 3 kpc instead of 1 kpc (§ I), the n_{H_2} derived from the $n_{13}L$ would be a factor of 3 lower, while n_{H_2} derived from H_2CO excitation would be unaffected. Thus the larger distance estimate would make the discrepancy worse. The largest possible source of error in determining $n_{13}L$ is the assumption of low optical depth. Cloud models were constructed, by using the LVG approximation, that reproduce the observed CO and ^{13}CO profiles; the optical depth of ^{13}CO was $\tau = 0.3$ even at the peak position. The other assumptions used to derive $n_{13}L$ were also verified. The remaining source of possible error is the relation between $n_{H_2}L$ and $n_{13}L$ (eq. [3]). These data indicate that, in the denser regions of the cloud where H_2CO emission is seen, the ratio of n_{H_2}/n_{13} must be substantially higher than the value in equation (3), which was derived from studies of dark clouds with $n_{13}L \lesssim 27 \times 10^{15}$ cm^{-2}. If this situation occurs commonly, the use of CO data alone to estimate the density and mass of molecular clouds could result in a large underestimate.

It is important to realize that the discrepancy between ^{13}CO and H_2CO results cannot be explained merely as an increased abundance of H_2CO. In fact the H_2CO abundance must be kept rather small ($\sim 3 \times 10^{-10}n_{H_2}$) in order to explain the very weak 2 cm line. This in turn necessitates a large hydrogen density which thermalizes both ^{12}CO *and* ^{13}CO. Thus only a small optical depth of ^{13}CO will explain the low $T_A{}^*$ of ^{13}CO relative to ^{12}CO. These arguments apply only to the region (3′–4′ in diameter) where H_2CO emission is seen. The mass inside a 1′ radius at $n_{H_2} = 2 \times 10^5$ cm^{-3} is 900 $M_\odot$, nearly half the total cloud mass estimated from ^{13}CO. The mass of the entire cloud calculated from ^{13}CO data above may not be greatly affected unless the same factors are at work farther out in the cloud. The most logical explanation is that molecules like CO and H_2CO are less abundant relative to H_2 in the dense portions of this, and perhaps other, molecular clouds than would be indicated by

Dickman's (1976) relation for dark clouds. A more detailed discussion of this question, applied to other clouds, will be published elsewhere.

To summarize, the H_2CO data indicate that high densities exist over a 3′–4′ region around the CO peak, the infrared source, and the H_2O and OH masers. At a density of 2×10^5 cm^{-3}, the mass inside a 1′ radius sphere is 900 $M_\odot$. This density conflicts strongly with that derived from ^{13}CO, suggesting that Dickman's relation between H_2 and ^{13}CO abundances breaks down in the dense regions of the cloud. Farther from the CO peak, where H_2CO emission cannot be seen, we are forced to rely on indirect measures of n_{H_2}. These indicate an average density of 800 cm^{-3}, which is consistent with the minimum density needed to explain the 6 cm absorption of H_2CO. Using these densities, we find that the mass of the cloud is 1.5×10^3 $M_\odot$. If the ^{13}CO is also depleted in these regions these may be underestimates, especially since the virial theorem yields 5×10^3 $M_\odot$ for the cloud.

V. THE ENERGETICS OF THE CLOUD

A study of the energetics of molecular clouds must ultimately deal with the relation between the gas and the dust. Collisions of gas molecules with dust grains are thought to be an important source of heat for the gas (Goldreich and Kwan 1974). Recent studies indicate that H_2O molecules may be an intermediary between dust and gas through absorption of far infrared radiation and collisional de-excitation with H_2 molecules (Scoville and Kwan 1976). In both these pictures, the dust provides a heat source for the gas and thus must be at a temperature higher than the gas kinetic temperature.

The study of far-infrared radiation from giant H II region–molecular cloud complexes has left unanswered several important questions (cf. Blair 1976). Among these questions are the location of the dust which produces the far-infrared emission, the ultimate energy source for the dust and gas emission, and the total luminosity of compact near-infrared objects. The data presented here on S255 and those presented by Blair *et al.* (1977) on S140, when combined with suitable far-infrared observations, should begin to provide some answers to these questions.

In this section we will discuss cooling and heating rates for the gas and dust in the molecular cloud. In discussing the energetics of the molecular cloud, it is necessary to recognize that the gas and dust form largely separate systems. The primary flow of energy for the cloud as a whole is through the dust; it absorbs the photons from nearby stars and embedded near-infrared sources and reradiates energy in the far-infrared. Because of the very low heat capacity of the gas relative to the grains, the dust energetics are largely independent of the gas energetics. In regions of high density the gas temperature (T_K) is coupled to the dust temperature (T_d) directly through inelastic collisions of dust and H_2. Other heat sources may play a role in the gas energetics, but dust *cooling* of gas is so effective

that we expect $T_d \geq T_K$ in dense, warm molecular clouds.

a) Cooling Rates for the Gas

The hydrogen gas is itself a very poor radiator at low temperatures because of its lack of a microwave or millimeter spectrum. Hence collisions with other molecular species transfer the energy, and radiation by those species cools the hydrogen gas.

At the temperature of typical molecular clouds, CO is the primary gas coolant. Although we observe only the $J = 1 \rightarrow 0$ line, the cooling rate due to radiation in the various CO lines may be computed from

$$\Lambda(\text{CO}) = 2 \times 10^{-27} T_K{}^3 \ (\text{ergs cm}^{-3} \text{ s}^{-1}) \quad (4)$$

given by Scoville and Solomon (1974). This formula is an analytic approximation to the cooling rate found by radiative-transport calculations; it is applicable at densities such that $n_{\text{CO}} n_{\text{H}_2} \gg 10^2 \text{ cm}^{-6}$. To compute the total cooling rate of the cloud, we have added the contribution of the concentric shells, using the T_K determined by means of equation (1), out to the shell defined by the 10 K contour of $T_A{}^*$. The contribution of each shell is given in column (6) of Table 5 as $\Lambda_{\text{CO}} \Delta v_i$, where Δv_i equals $v_i - v_{i-1}$. The resulting total gas cooling rate is

$$\sum_i \Lambda_i(\text{CO}) \Delta v_i = 2.5 \, L_\odot .$$

This cooling rate is much less than any plausible estimate of the total dust cooling rate.

b) Heating Rates of the Gas

The total energy radiated by CO ($2.5 \, L_\odot$) is far less than either the energy radiated by dust or the available energy inputs. However, the gas requires a heating rate per unit volume equal to its cooling rate (Λ_{CO}) in order to maintain T_K at its observed value.

Models for heating the gas by inelastic collisions of gas molecules and dust grains require that $T_d \sim 2T_K$ at $n_{\text{H}_2} = 10^4 \text{ cm}^{-3}$. In a model with H_2O acting as the intermediary, the gas heating rate depends on the H_2O/H_2 ratio as well as n_{H_2} and T_d, but for a favorable case Scoville and Kwan (1976) find that T_K may be $\frac{3}{4} T_d$ at $n_{\text{H}_2} = 10^4 \text{ cm}^{-3}$. Because both these models will imply large far-infrared luminosities for the cloud, other possible heat sources for the gas should be considered.

The rate of compressional heating due to collapse may be calculated from $H_{\text{comp}} = n_{\text{H}_2} k T_K / \tau_{\text{ff}}$, where τ_{ff} is the free-fall collapse time. Then to maintain the gas at T_K, neglecting the dust, $H_{\text{comp}} = 1.2 \times 10^{-31} n_{\text{H}_2}{}^{3/2} T_K$ must equal $\Lambda_{\text{CO}} = 2 \times 10^{-27} T_K{}^3$, which leads to the requirement that $n_{\text{H}_2} = 650 T_K{}^{4/3}$. For example, at $T_K = 30$ K, $n_{\text{H}_2} = 6 \times 10^4$; at $T_K = 15$ K, n_{H_2} must be 2.5×10^4. Thus compressional heating could maintain T_K at the values observed *in the dense portion* of the cloud, if the cooling due to dust is neglected. However, in these dense regions, the gas-dust collision time $t_c = 4.5 \times 10^{16} n_{\text{H}_2}{}^{-1} T_K{}^{-1/2}$ s

(Goldreich and Kwan 1974) is shorter than the free-fall time $\tau_{\text{ff}} = 1.15 \times 10^{15} n_{\text{H}_2}{}^{-1/2}$ s; thus the dust cannot be neglected in the gas energetics.

While there may be still other sources of gas heating, the above argument implies that the dust cannot be ignored. Collisions with dust are expected to *cool* the gas rapidly if $T_K > T_d$ (Scalo 1977). Thus one is forced to assume that the dust temperature is at least equal to the gas temperature in much of the cloud. Other heat sources could still be important in the sense that they allow $T_d = T_K$, whereas the dust heating model requires $T_d > T_K$ by factors which are often 2 or more. Because the dust emission depends on a high power of T_d, the predicted far-infrared flux from the cloud will be rather sensitive to how close T_K may be to T_d.

If the density drops to 10^3 cm^{-3} away from the molecular peak, as indicated by the ^{13}CO data, then neither compressional heating nor dust heating is very effective at maintaining T_K at the observed values of 15–20 K. Other heat sources may have to be considered for this region once T_d and n_{H_2} have been determined over substantial parts of molecular clouds.

c) Cooling Rates for the Dust

The dust cooling rates could be determined directly if maps of far-infrared emission were available. Because this information is at present lacking, the CO observations will be used to provide a rough estimate of the far-infrared emission. Using the surface areas $s_i = 4a_i$ defined above out to the 10 K contour of $T_A{}^*(\text{CO})$, taking $T_d = T_K$ for each ring, and taking the cooling equal to $\sigma T_d{}^4 s_i$ (blackbody emission), we find a dust cooling rate of $1.7 \times 10^6 L_\odot$. The geometrical assumption introduces a possible error of about a factor of 2. The assumption of blackbody emission is not likely to be right, however, as most molecular clouds are not optically thick throughout the far-infrared.

To achieve a better estimate of the dust cooling, an estimate is needed of the average optical depth in the far-infrared, τ_{FIR}. As outlined in the Appendix, we have chosen to use $n_{13}L$ as an indicator of τ_{FIR}. The empirical relation

$$\tau_{\text{FIR}} \approx 10^{-18} n_{13} L \quad (5)$$

was found to apply to the data on most molecular clouds within a factor of 2. However, we do not consider equation (5) to be more than a rough guideline.

From the value of $n_{13}L = 3.7 \times 10^{16} \text{ cm}^{-2}$ at the CO peak, we find $\tau_{\text{FIR}} = 0.037$. A value of $n_{13}L$ averaged over the region of $T_A{}^*(\text{CO}) > 20$ K yields $\tau_{\text{FIR}} = 0.02$. The cooling rates from each shell $[C_i(\text{FIR})]$ are given in Table 5, using $\tau_{\text{FIR}} = 0.037$ for the inner shell and $\tau_{\text{FIR}} = 0.02$ for all others. These are lower limits in the sense that we have assumed $T_d = T_K$. While this may be close to correct in the denser regions, T_d may be significantly greater than T_K farther out in the cloud. The total cooling rate

$$\sum_i C_i(\text{FIR}) = 3.5 \times 10^4 L_\odot .$$

It should be noted that the region responsible for most of the cooling is that with $T_A{}^*(\text{CO}) = 15–20$ K.

The high-temperature peak $[T_A^*(CO) = 30\,K]$ contributes a factor ~ 3 less cooling because of its much smaller surface area compared with the region of $T_A^*(CO) = 20\,K$. For a cloud heated by a single internal heat source, one would expect each shell to have the same luminosity. The cooling rates in Table 5 suggest that more than one heat source is affecting the cloud, a suggestion which is supported by the following discussion of heating rates for the dust.

d) Heating Rates for the Dust

We first consider heating by the embedded source S255 IR. The *observed* luminosity, uncorrected for attenuation, of S255 IR is obtained by integrating the energy distribution of Figure 5. The result is $620\,L_\odot$, in good agreement with the data of Pipher and Soifer (1976). This is considered as a heat input to the cloud for the following reason. From detailed considerations of other sources of this type, it is clear that the radiation at $\lambda > 5\,\mu m$, where the bulk of the energy in the observed spectrum lies, cannot be reddened starlight (Becklin, Neugebauer, and Wynn-Williams 1973; Beckwith *et al.* 1976). The radiation must instead be due to thermal radiation by dust which may be heated by a stellar core. The exact nature of the source does not concern us; for our purposes, it suffices to note that the observed radiation implies that an equal amount of energy has been deposited in the dust in the cloud.

The observed radiation is a lower limit to the object's luminosity because the silicate feature indicates that some absorption has taken place between the region emitting at $10\,\mu m$ and the outside of the cloud. Pipher and Soifer (1976) calculate that $3.5 \times 10^3 < L/L_\odot < 5 \times 10^3$, based on their measurements of the silicate feature and a distance of 1 kpc. These corrections are large and must be considered uncertain owing to the fact that the opacity law of the grains is poorly known at these wavelengths. If this energy is absorbed by grains farther from the primary source (and hence cooler grains), it represents a heat input and should appear as far-infrared radiation. We note that the largest estimate is a factor of 7 too low to account for the total predicted far-infrared luminosity of $3.5 \times 10^4\,L_\odot$, but would account for the luminosity predicted for the region of the highest CO temperatures. The errors involved in estimating the luminosity of S255 IR, and especially the errors involved in predicting the far-infrared luminosity, are sufficiently large that S255 IR could still have sufficient energy to account for the far-infrared emission.

Next we consider heating of the dust in the cloud by the exciting stars of the nearby H II regions. There are four stars of types B0 to O9.5 in the vicinity of the molecular cloud. Because the CO cloud does not extend behind the S254 region, the exciting star of that H II region will be ignored in the following discussion. The exciting stars of S255, S256, and S257 all have spectral type B0, which implies a luminosity $\sim 5 \times 10^4\,L_\odot$ (Panagia 1973). If all the energy from these exciting stars (i.e., $\sim 1.5 \times 10^5\,L_\odot$) were available to

heat the cloud, then the effect of S255 IR on the *overall* energetics of the cloud would clearly be negligible. Because the cloud does not extend in front of the nebulae, no more than half this radiation is available. Furthermore, the transfer of radiation from an external source into a molecular cloud is poorly understood, and it is not clear how much energy would actually go into heating the cloud. The dust cooling rate calculated in § Vc would be balanced by heating if a fraction 0.2 of the stellar radiation actually heated the cloud.

e) Summary

Based on their luminosity and apparent location with respect to the cloud, the exciting stars of the nearby H II regions appear to provide the main energy source for the cloud. These stars have sufficient luminosity to account for the estimated far-infrared radiation by dust. The luminosity of the near-infrared source S255 IR, when corrected for silicate absorption (Pipher and Soifer 1976), is not sufficient to balance the total inferred dust cooling rate, but it can balance the inferred dust cooling rate for the region around the CO peak. The total gas cooling rate by radiation in the CO lines is extremely small compared with the dust cooling rate. Consideration of gas *cooling* by dust implies that $T_d \geq T_K$, and if the gas is *heated* by the dust, then $T_d > 1.3\text{--}2.0T_K$. We consider the observational consequences of the picture developed here in the next section.

VI. OBSERVATIONAL CONSEQUENCES

The estimate of the dust cooling rate in § V is subject to serious uncertainties. Direct measurements of the dust emission are very desirable. To determine the feasibility of such measurements, we will use the estimate in § V to predict the infrared flux to be expected from the cloud. If the total dust cooling rate of $3.5 \times 10^4\,L_\odot$ is radiated over a bandwidth of 10^{13} Hz in the far-infrared, the flux observed from the whole cloud would be 1.2×10^4 Jy. This value is uncertain because τ_{FIR} is uncertain and because we have assumed $T_d = T_K$; if $T_d = 2T_K$, then the predicted cooling rate and flux would be 16 times larger.

Despite the very large predicted flux, direct observations may not be trivial for two reasons. The first is that the predicted emission is very extended and will have a low surface brightness over most of the cloud. The second reason is that the dust temperature may be low enough so that most of the emission is at very long wavelengths. For example, the flux from dust at 30 K would peak at $160\,\mu m$ and the flux from 15 K dust would peak at $320\,\mu m$. To evaluate the importance of these effects, we have computed the expected flux for several observing situations. Table 6 presents the flux into a 1' beam predicted from a region centered on the peak and from a region away from the peak but within the $T_A^*(CO) > 20\,K$ region. Predictions are presented for $\lambda = 100\,\mu m$ and $\lambda = 350\,\mu m$ for the two situations, $T_d = T_K$ and $T_d = 2T_K$. The τ at $100\,\mu m$ is determined from equation (5) and the τ at $350\,\mu m$

TABLE 6

PREDICTED FLUXES INTO A 1' BEAM

Position	T_d (K)	S_ν (100 μm) (Jy)	S_ν (350 μm) (Jy)
Peak position............	34	1450	553
	68	1.4×10^4	1560
Away from peak ($n_{13}L = 2 \times 10^{16}$)........	24	133	154
	48	2800	517

from the relation given by Righini-Cohen and Simon (1977). It is clear from Table 6 that the molecular peak should be observable even if $T_d = T_K$, but that emission away from the peak will be quite weak at 100 μm if $T_d = T_K$. The predicted flux from the peak may actually be an underestimate if the temperatures continue to rise around the near-infrared source on a scale less than 1'. An unresolved, high-temperature core will have a much greater effect on the dust emission than on the CO emission.

The remaining question is why does the CO intensity, hence T_K and presumably T_d, peak where it does? The exciting stars of the H II regions appear to be supplying most of the heat for the cloud, and the CO map indicates that molecular gas extends behind the H II region S255 and at least the eastern part of S257 and S256. Furthermore, the appearance of the 21 cm radio map suggests that dense gas exists between S255 and S257, as illustrated in the model of Figure 7. Under these conditions, a CO peak might have been expected behind the H II regions or along

the boundary of the H II region and molecular cloud. Instead, the CO data with high spatial resolution confirm that the CO peak is closer to S255 IR than to the edge of S255, and no peaking is observed behind the H II regions. With the geometry of Figure 7, the exciting star of S255 would supply an input of 680 $L_\odot$ to a 1' diameter region around the CO peak. This estimate is an upper limit because it assumes no attenuation between the star and the CO peak. Thus it is quite reasonable that the heating from the infrared source can dominate heating by the exciting stars over a small region near the infrared source, even if the exciting stars dominate the overall heating of the cloud. Finally, the lack of CO peaks around the boundaries of the H II regions may be due to destruction of molecules close to the boundary. If this explanation is correct, one may still expect to see strong far-infrared emission from the boundary regions indicating the presence of hot dust without the accompanying hot CO. Such an observation would not damage the picture of cloud energetics developed in this paper, since we have dealt only with the far-infrared and submillimeter flux that is implied by the molecular emission and the assumption that $T_d \geq T_K$. The techniques used here are not expected to give a good estimate of the far-infrared emission from the H II region and its boundaries, or from the immediate vicinity of a near-infrared source. The test of the cloud energetics picture is to measure T_d at positions away from the H II region and near-infrared source. If $T_d < 1.3T_K$, then current models in which the gas is heated by dust have to be reconsidered. If $T_d < T_K$,
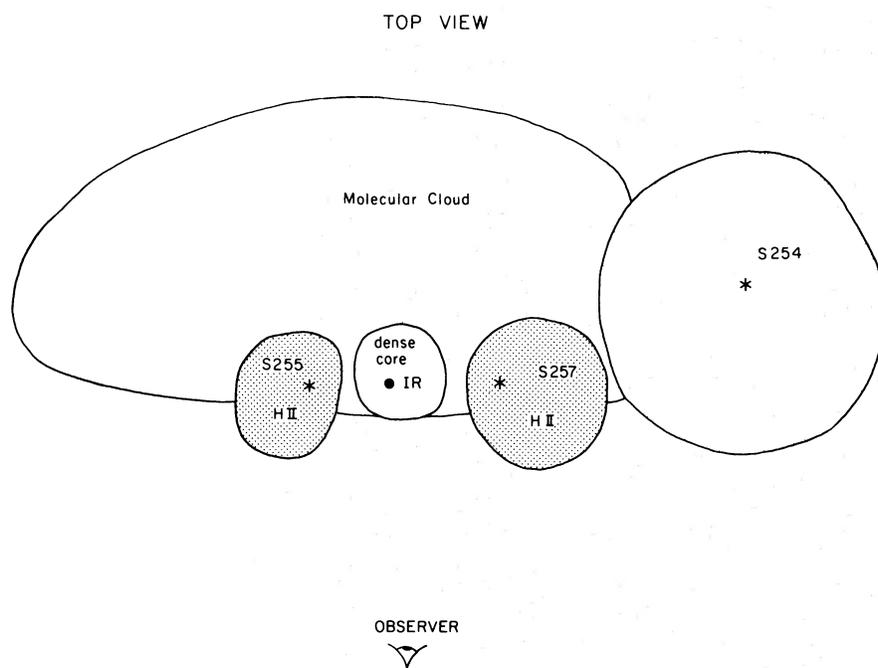

FIG. 7.—A schematic model of the molecular cloud–H II region. A top view is presented to illustrate the probable presence of dense gas between the two H II regions, S255 and S257, and the extension of the molecular cloud behind the two H II regions. The extent of the dense core back into the cloud and the location of the IR source along the observer line of sight are unknown; the portrayal of these features in this figure is arbitrary.

then the gas-dust coupling must be questioned, and different gas heating sources would have to be considered.

VII. CONCLUSIONS

We have presented observations of the S255 molecular cloud in the radio lines of CO, ^{13}CO, and H_2CO and in the infrared region from 1.2 to 20 μm. The most important observational results are the following. An extended molecular cloud is associated with the optically visible H II regions, S255–S257. There is an enhancement of both kinetic temperature and molecular density centered on a compact near-infrared source. This infrared source is also coincident within the errors with an OH and an H_2O maser, but no radio continuum source greater than 3 mJy at 6 cm is coincident with the source. The infrared source peaks around 5–20 μm and exhibits the silicate absorption feature.

We have also presented first-order techniques which allow estimates of the physical properties of molecular clouds and analysis of the energetics of the gas and dust in the clouds. Application of these techniques to the S255 molecular cloud results in the following conclusions. The gas cooling rate is much less than the dust cooling rate, and the primary flow of energy is in the infrared through dust emission at a range of temperatures. These conclusions are based on the argument that the dust temperature must at least equal the gas kinetic temperature and on an empirical relation between the far-infrared optical depth of the dust and the column density of ^{13}CO. The near-infrared source is apparently responsible for the local peak in gas kinetic temperature, but published estimates of the luminosity of the near-infrared source are not sufficient to balance the total predicted dust emission from the extended cloud. The exciting stars of nearby H II regions appear to be the primary heat sources for the overall molecular cloud.

In this cloud, as in the Orion Molecular Cloud, both an infrared source and the exciting stars of H II regions provide an energy input for the molecular cloud. In the S255 molecular cloud, the luminosities of stars and infrared sources, and the cloud mass and temperature, are all less than the corresponding values in Orion and more typical of observed molecular clouds. A more favorable geometry exists in this cloud as well; an important feature is that the H II regions are sharply confined and there are suitable points in the molecular cloud where T_K is still substantial but there is no ionized gas along the line of sight. The infrared source is clearly distinct from the H II regions, and careful measurements in the far-infrared may be able to check the large bolometric corrections suggested by analysis of the silicate feature. However, a better source in this respect is the S140 molecular cloud, which will be reported in another paper of this series (Blair *et al.* 1977). The principal virtue of the S255 source is the existence of a fairly extensive, warm molecular cloud with no H II regions or infrared sources along many lines of sight. This allows a clean test of the contention that $T_d \geq T_K$ and the relation between the far-infrared optical depth of dust and the molecular column density. Far-infrared fluxes have been predicted for suitable test cases. Measurements in the far-infrared which determine T_d and τ_{FIR} would allow improvement of the first-order analysis employed here and extension of improved analysis to clouds where tests are more difficult. If the far-infrared fluxes are substantially below the predictions of this paper, then basic aspects of cloud energetics must be reconsidered.

APPENDIX

Many authors (e.g., Fazio and Stecker 1976) have attempted to relate the ^{12}CO column density ($n_{12}L$) to τ_{FIR}. We believe that this is dangerous because $n_{12}L$ is not directly obtained from the data; ^{12}CO emission is optically thick and must be calculated from the ^{13}CO column density ($n_{13}L$) by using an assumption about the CO/^{13}CO abundance in molecular clouds, the latter being a subject of considerable controversy (see, e.g., Wannier 1975, or Watson, Anicich, and Huntress 1976). Furthermore, if $n_{H_2} \approx 10^3$, the optically thick CO line is affected greatly by radiative trapping (Goldreich and Kwan 1974; Scoville and Solomon 1974), and one will tend to underestimate the true column density.

Because the ^{13}CO line is generally optically thin, we have chosen to use $n_{13}L$ to estimate the value of τ_{FIR} from data on other sources. As noted above, the uncertainty in determining $n_{13}L$ from $T_A*(^{13}CO)$ is no more than a factor of 2 as long as the ^{13}CO is optically thin. In cases where the ^{13}CO may not be thin, we have used the column density of $^{12}C^{18}O$ and multiplied by 14.3 (Wannier *et al.* 1976) to get $n_{13}L$. The difficulty is in relating $n_{13}L$ to τ_{FIR}. Theoretical approaches must assume gas-to-dust ratios, the fraction of C in CO, and the grain opacity in the far-infrared (see Fazio and Stecker 1976). The last quantity is especially uncertain and, as we have seen in § IV*c*,

the fraction of C in CO may also be uncertain. Therefore we have sought an empirical relation between $n_{13}L$ and τ_{FIR} by using the available data on well-studied molecular clouds. The techniques used to estimate τ_{FIR} vary, depending on the nature of the data. The best technique is to determine the far-infrared color temperature and compare it with the brightness temperature. This particular technique has been applied to obtain τ_{FIR} from far-infrared observations of a variety of sources (Harvey, Hoffmann, and Campbell 1975; Harvey, Campbell, and Hoffmann 1977).

A less satisfying technique is sometimes used when only broad-band observations ($\lambda \sim 40$ to $350\,\mu$m) are available. By assuming that $T_d = T_K$, we may infer τ_{FIR} by the ratio of observed emission to that expected from a blackbody at temperature T_K. This technique was applied to the data on NGC 2023 (Emerson, Furniss, and Jennings 1975) and W3 (Furniss, Jennings, and Moorwood 1975).

The relationship expressed in equation (5) fits most of the available data within a factor of 2. (The two exceptions are W49 and W51; in both of these sources, estimates of $n_{13}L$ by different observers differ by an order of magnitude.) That the two different methods, applied to different clouds, agree so well is encouraging; but at present we do not consider equation (5) to be more than a rough guideline. A similar approach has been used to determine $\tau_{350\,\mu m}$ and $\tau_{1\,mm}$ relative to $n_{13}L$ (Righini-Cohen and Simon 1977), with results generally consistent with the above relation.

Note added in manuscript.—While this paper was in the editing stages, the evidence for a distance of 2–3 kpc was strengthened. We consider briefly the effect on some of the derived quantities of assuming a distance of 2.5 kpc. There would be no change in the predicted far-infrared fluxes (Table 6), the luminosities of nearby stars, the kinetic temperatures, the ^{13}CO column densities, or the hydrogen densities derived from formaldehyde excitation. The hydrogen densities derived from the ^{13}CO column densities would decrease, sharpening the discrepancy with the formaldehyde results. This development would strengthen the case for a lower CO abundance in this cloud, as compared with dark clouds. The mass determined from ^{13}CO, the predicted dust cooling rate, and the luminosity of S255 IR would all increase by a factor of 6.25. These changes would make it somewhat difficult to balance the dust cooling rate with the heating from nearby stars. Also S255 IR would play a greater role in the overall energetics, because its luminosity would now be comparable with that of one of the stars exciting the H II regions. Finally, the gas cooling rate, and the mass in the formaldehyde emission core, would be multiplied by 15.6. In this case, the mass in the dense core would exceed the total mass estimate from ^{13}CO; however, the uncertainties in the core mass are large because it depends heavily on the assumption of spherical symmetry. The gas cooling rate would still be much smaller than the predicted dust cooling rate, and the arguments in § Vb on gas heating would not be affected. All in all, a larger distance for the cloud would not alter the basic conclusions of this paper, but it would strengthen the case for a low CO abundance in this cloud.

REFERENCES

Becklin, E. E., Neugebauer, G., and Wynn-Williams, C. G. 1973, *Ap. J. (Letters)*, **182**, L7.
Beckwith, S., Evans, N. J., II, Becklin, E. E., and Neugebauer, G. 1976, *Ap. J.*, **208**, 390.
Blair, G. N. 1976, Ph.D. thesis, University of Texas at Austin.
Blair, G. N., Evans, N. J., II, Vanden Bout, P. A., and Peters, W. L. 1977, in preparation.
Blair, G. N., Peters, W. L., and Vanden Bout, P. A. 1975, *Ap. J. (Letters)*, **200**, L161.
Dickman, R. L. 1976, Ph.D. thesis, Columbia University.
Emerson, J. P., Furniss, I., and Jennings, R. E. 1975, *M.N.R.A.S.*, **172**, 411.
Evans, N. J., II, Crutcher, R. M., and Wilson, W. J. 1976, *Ap. J.*, **206**, 440.
Evans, N. J., II, and Kutner, M. L. 1976, *Ap. J. (Letters)*, **204**, L131.
Evans, N. J., II, Zuckerman, B., Sato, T., and Morris, G. 1975, *Ap. J.*, **196**, 433.
Fazio, G. G., and Stecker, F. W. 1976, *Ap. J. (Letters)*, **207**, L49.
Furniss, I., Jennings, R. E., and Moorwood, A. F. M. 1975, *Ap. J.*, **202**, 400.
Goldreich, P., and Kwan, J. 1974, *Ap. J.*, **189**, 441.
Harvey, P. M., Campbell, M. F., and Hoffmann, W. F. 1977, *Ap. J.*, **211**, 786.

Harvey, P. M., Hoffmann, W. F., and Campbell, M. F. 1975, *Ap. J. (Letters)*, **196**, L31.
Israel, F. P. 1976, *Astr. Ap.*, **51**, 175.
Kutner, M. L., Evans, N. J., II, and Tucker, K. D. 1976, *Ap. J.*, **209**, 452–461.
Leung, C. M. 1976, *Ap. J.*, **208**, 732.
Lo, K. Y., and Burke, B. F. 1973, *Astr. Ap.*, **26**, 487.
Panagia, N. 1973, *A.J.*, **78**, 929.
Pipher, J. L., and Soifer, B. T. 1976, *Astr. Ap.*, **46**, 153.
Righini-Cohen, G., and Simon, M. 1977, preprint.
Scalo, J. M. 1977, *Ap. J.*, **213**, 705.
Scoville, N. Z., and Kwan, J. 1976, *Ap. J.*, **206**, 718.
Scoville, N. Z., and Solomon, P. M. 1974, *Ap. J. (Letters)*, **187**, L67.
Sharpless, S. 1959, *Ap. J. Suppl.*, **4**, 257.
Strom, K. M., Strom, S. E., and Vrba, F. J. 1976, *A.J.*, **81**, 308.
Turner, B. E. 1971, *Ap. Letters*, **8**, 73.
Wannier, P. G. 1975, Ph.D. thesis, Princeton University.
Wannier, P. G., Penzias, A. A., Linke, R. A., and Wilson, R. W. 1976, *Ap. J.*, **204**, 26.
Watson, W. D., Anicich, V. G., and Huntress, W. T., Jr. 1976, *Ap. J. (Letters)*, **205**, L165.
Zuckerman, B., and Evans, N. J., II. 1974, *Ap. J. (Letters)*, **192**, L149–L152.

S. Beckwith: Department of Physics, California Institute of Technology, Pasadena, CA   91125

Guy N. Blair: Radiosterrenwacht, Dwingeloo, The Netherlands

N. J. Evans, II: Department of Astronomy, University of Texas, Austin, TX   78712